
The Impact of Non-stationarity on Generalisation in Deep Reinforcement Learning

Maximilian Igl *

Gregory Farquhar *,†

Jelena Luketina *

Wendelin Böhmer *

Shimon Whiteson *

Abstract

Non-stationarity arises in Reinforcement Learning (RL) even in stationary environments. Most RL algorithms collect new data throughout training, using a non-stationary behaviour policy. Furthermore, training targets in RL can change even with a fixed state distribution when the policy, critic, or bootstrap values are updated. We study these types of non-stationarity in supervised learning settings as well as in RL, finding that they can lead to worse generalisation performance when using deep neural network function approximators. Consequently, to improve generalisation of deep RL agents, we propose Iterated Relearning (ITER). ITER augments standard RL training by repeated knowledge transfer of the current policy into a freshly initialised network, which thereby experiences less non-stationarity during training. Experimentally, we show that ITER improves performance on the challenging generalisation benchmarks *ProcGen* and *Multiroom*.

1 Introduction

This paper addresses generalisation to states not seen during training with RL, which is critical to tackle many diverse real-world applications. As in most machine learning settings, generalisation may be improved in RL by collecting more data and ensuring its diversity [Cobbe et al., 2019b]. Furthermore, many regularisation methods developed for Supervised Learning (SL) can be made effective in RL [Igl et al., 2019]. In this paper, we instead focus on *non-stationarity* as a potential cause of poor generalisation, in particular in deep RL, when we rely on neural networks as function approximator.

Non-stationarity arises in RL for at least three reasons. First, the behaviour policy usually changes during training, affecting the state-action distribution of the data we learn from. Second, we often try to learn the value function of a constantly changing policy. Lastly, when we use temporal difference methods [Sutton, 1988] to learn the value of even a fixed policy, the bootstrap values induce a moving target for regression which in turn also affects the policy gradient estimator. Similar types of non-stationarity can arise in SL as well. For example, additional training data might be added over time, sometimes from a changing data distribution as in active learning [Settles, 2009]. Additionally, the labelling process might be changed or refined over time, moving the learning targets.

In deep RL, this non-stationarity is often not addressed explicitly. Typically, a single neural network model is initialised and continually updated during training. Conventional wisdom about catastrophic forgetting [Kemker et al., 2018] implies that old updates from a different data- or target- distribution will simply be forgotten. However, we provide evidence for an alternative hypothesis: continual updates to a model in the presence of certain types of non-stationarity can harm generalisation.

We first study this phenomenon in artificially constructed supervised settings using the CIFAR-10 dataset. While training performance is nearly unaffected by the non-stationarity we induce, test

*University of Oxford. Corresponding author: Maximilian Igl (maximilian.igl@gmail.com)

†Now at DeepMind, London

performance degrades considerably. This shows that early network updates can have a lasting negative impact on the generality of the learned model. While the importance of early training phases is already known for factors such as regularisation [Golatkar et al., 2019] and hyper-parameters [Frankle et al., 2020], in this paper we investigate the impact of a changing data distribution.

We then consider the RL setting, where such non-stationarities are common. Consequently, it is important for the optimal generalisation of trained RL agents to reduce the dependence on early training. To do so, we propose ITER. In this paradigm, the knowledge from an agent is periodically distilled into a freshly initialised student, using data drawn from the latest agent’s policy. This reduces the amount of non-stationarity faced by the student, helping it to learn and use representations that generalise well across the entire state-action distribution. Eventually, the student replaces the teacher and the cycle repeats. We can perform this distillation in parallel to the training process (see fig. 1), without requiring additional training data. Experimentally, we evaluate ITER on the fully observable *Multiroom* environment, as well as several environments from the recently proposed partially observable *ProcGen* benchmark, and find that it indeed improves generalisation.

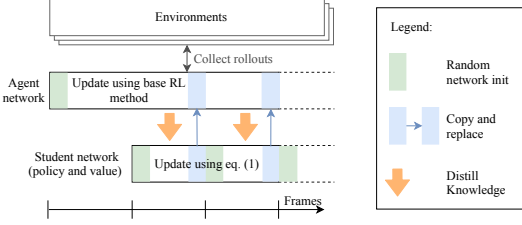


Figure 1: The ITER *agent* interacts with the environment and is trained by the base RL method. The *student* is *randomly initialised* and learns for some time in parallel to imitate the ITER agent, after which the agent is *replaced* by the student and the cycle repeats. We show that this improves generalisation, as the student’s training data exhibits much less non-stationarity.

2 Background

We describe an RL problem as a Markov decision process (MDP) $(\mathcal{S}, \mathcal{A}, T, r, p_0, \gamma)$ [Puterman, 2014] with actions $a \in \mathcal{A}$, states $s \in \mathcal{S}$, initial state $s_0 \sim p_0$, transition dynamics $s' \sim T(s, a)$, reward function $r(s, a) \in \mathbb{R}$ and discount factor γ . The unnormalised discounted state distribution induced by a policy π is defined as $d_\pi(s) = \sum_{t=0}^{\infty} \gamma^t \Pr(S_t = s | S_0 \sim p_0, A_t \sim \pi(\cdot | S_t), S_{t+1} \sim T(S_t, A_t))$. In ITER, we learn a sequence of policies and value functions, which we denote with $\pi^{(k)}(a|s)$ and $V^{(k)}(s)$ at the k th iteration ($k \in \{0, 1, 2, \dots\}$), parameterized by θ_k .

We briefly discuss some forms of non-stationarity which can arise in RL, even when the environment is stationary. For simplicity, we focus the exposition on actor-critic methods which use samples from interaction with the environment to estimate the policy gradient given by $g = \mathbb{E}[\nabla_{\theta} \log \pi_{\theta}(a|s) A^{\pi}(s, a, s') | s, a, s' \sim d_{\pi}(s) \pi(a|s) T(s', a)]$. The advantage is often estimated as $A^{\pi}(s, a, s') = r(s, a) + \gamma V^{\pi}(s') - V^{\pi}(s)$. Typically, we also use neural networks to approximate the baseline $V_{\phi}^{\pi}(s)$ and for bootstrapping from the future value $V_{\phi}^{\pi}(s')$. ϕ can be learned by minimising $\mathbb{E}[A^{\pi}(a, s)^2]$ by stochastic semi-gradient descent, treating $V_{\phi}^{\pi}(s')$ as a constant.

There are at least three main types of non-stationarity in deep RL. First, we update the policy π_{θ} , which leads to changes in the state distribution $d_{\pi_{\theta}}(s)$. For example, early on in training, a random policy π_{θ} only explores states close to initial states s_0 . As π_{θ} improves, new states further from s_0 are encountered. Second, changes to the policy also impact the observed rewards, changing the true value function $V^{\pi}(s)$ which $V_{\phi}^{\pi}(s)$ is approximating. Lastly, due to the use of bootstrap targets in temporal difference learning, the learned value $V_{\phi}^{\pi}(s)$ is not regressed directly towards $V^{\pi}(s)$. Instead V_{ϕ}^{π} fits a gradually evolving target sequence even under a fixed policy π , thereby also changing the policy gradient estimator g .

3 The Impact of Non-stationarity on Generalisation

To demonstrate that non-stationarity in training impedes generalisation, we show in a set of Supervised Learning (SL) experiments that different non-stationarities have negative effects on the test performance of the final model, even though training accuracy is hardly affected.

In these experiments, carried out on the CIFAR10 dataset for image classification [Krizhevsky et al., 2009], we do not aim for optimal performance. Instead, we intend to create settings with important similarities to standard approaches in deep RL. We use a ResNet18 [He et al., 2016] architecture, similar to those used by Espeholt et al. [2018] and Cobbe et al. [2019a]. Following standard practice in RL, we use a constant learning rate and do not use batch normalisation. As in RL experiments on the *ProcGen* environment, we do use weight decay.

We train for a total of 2500 epochs. While the last 1500 are trained on the full, unmodified dataset, we introduce three different non-stationarities during the first 1000 epochs. Each is motivated by the RL setting. An exploring and improving policy typically observes a larger and larger part of the state-action space. To mimic this, the `Dataset Size` non-stationarity begins with a small fraction of the full dataset, and gradually adds additional data points after each epoch, at a constant rate, until the full dataset is available. In the non-stationary phase, data points are duplicated to ensure the same number of network updates are made in each epoch.

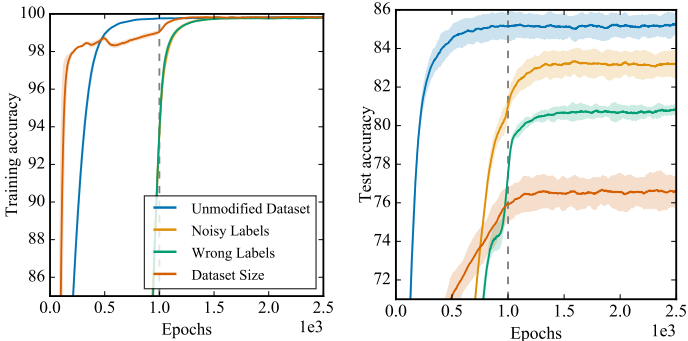


Figure 2: Accuracy on CIFAR-10 when the training data is non-stationary over the first 1000 epochs (dashed line). While final training performance (left) is almost unaffected, test accuracy (right) is significantly reduced.

Training targets in RL can also be non-stationary. A critic can introduce a temporally consistent bias in the estimate of the policy gradient, which may reduce in size as the critic improves. To imitate this effect, the `Wrong Labels` non-stationarity starts training with randomly drawn incorrect labels. After each epoch, a constant number of these labels are replaced with the correct ones. A poor critic or a highly stochastic initial policy could also introduce additional variance into the policy gradient estimates. The corresponding `Noisy Labels` non-stationarity is similar to `Wrong Labels`, but the incorrect labels are sampled uniformly at the start of each epoch.

The results are shown in fig. 2. While the final training accuracy (left) is almost unaffected (see table 1 in the appendix for exact results), all three initial non-stationarities significantly reduce the test accuracy (right). The plateau in accuracy shows that this effect persists even after the models are further trained for many epochs using the full dataset with correct labels: non-stationarity early in training has a lasting effect on the learned representations and quality of generalisation. The effect is largest for `Dataset Size`. While all three types of non-stationarity are exposed to the same number of correct training data points at each epoch, `Dataset Size` has the least *variety* in observed inputs. This seems to lead to a particularly harmful long-lasting overfitting effect. In contrast, the effect is smallest for `Noisy Labels`. Adding noise during training can often have a regularising effect, which may mitigate the impact of the non-stationarity.

We present additional details and experiments in section 5.1, but turn now to the RL setting. There, we expect to encounter all of these types of non-stationarity, which may similarly cause poor generalisation.

4 ITER

In section 3, we have seen evidence that types of non-stationarity present in many deep RL algorithms can lead to impaired generalisation. To mitigate this, we propose Iterated Relearning (ITER). Instead of representing the agent with a single model that is continually updated through the entire training process, ITER learns a sequence of models, each of which is exposed to less non-stationarity and thereby generalises better. This idea can be applied on top of a wide range of base RL training methods. For simplicity, we focus in the following exposition on actor-critic methods and use Proximal Policy Optimization (PPO) [Schulman et al., 2017] for the experimental evaluation.

The underlying insight behind ITER is that while the representation of our agent might be significantly damaged by non-stationarity, the outputs of the agent on the training data are comparatively unaffected. Consequently, ITER aims to *re-learn* the current policy on the latest data, but without the non-stationarity induced by the initial training. As we show, this leads to representations that generalise better.

ITER begins with an initial policy $\pi^{(0)}$ and value function $V^{(0)}$ and then repeats the following steps, starting with iteration $k = 0$.

1. Use the base RL algorithm to train $\pi^{(k)}$ and $V^{(k)}$.
2. Initialise new *student* networks for $\pi^{(k+1)}$ and $V^{(k+1)}$. We refer to the current policy $\pi^{(k)}$ and value function $V^{(k)}$ as the *teacher*.
3. Distill the teacher into the student. This phase is discussed in more detail in section 4.1.
4. The student replaces the teacher: $\pi^{(k)}$ and $V^{(k)}$ can be discarded.
5. Increment k and return to step 1. Repeat as many times as needed.

This results in alternating RL training with distillation into a freshly initialised student. The RL training phases continue to introduce non-stationarity until the models converge, so we want to iterate the process, repeating steps 1-4. How often we do so depends on the environment and algorithm details and can be chosen as a hyper-parameter. In practice, the distillation phase and the subsequent RL training phase can also be carried out in parallel to improve sample efficiency. We discuss the relevant trade-offs in section 4.2.

4.1 Distillation Loss

Our goal during the distillation phase (step 3) is to learn a new student policy $\pi^{(k+1)}$ and value function $V^{(k+1)}$ that imitate the current teacher ($\pi^{(k)}, V^{(k)}$). If the student and teacher share the same network architecture, the student could of course imitate the teacher exactly by copying its parameters. However, since the teacher was trained under non-stationarity, its generalisation performance is likely degraded (see section 3). Consequently, we want to instead train a freshly initialised student network to mimic the teacher’s *outputs* for the available data, but learn a better internal representation by training on a *stationary* data distribution. To achieve this, we use data generated by the teacher $\pi^{(k)}$, i.e., $s, a \sim d_{\pi^{(k)}}(s)\pi^{(k)}(a|s)$, instead of letting the student directly interact with the environment to collect data.

The student, parameterised by θ_{k+1} , is trained using a linear combination of four loss terms:

$$\mathcal{L}(\theta_{k+1}) = \alpha_\pi \mathcal{L}_\pi + \alpha_V \mathcal{L}_V + \mathcal{L}_{\text{PG}} + \lambda_{\text{TD}} \mathcal{L}_{\text{TD}} \quad (1)$$

where λ_{TD} is a fixed hyper-parameter and we linearly anneal α_π and α_V from some fixed initial value to zero over the course of each distillation phase.

\mathcal{L}_π and \mathcal{L}_V are supervised losses minimising the disagreement between outputs of the student and the teacher:

$$\begin{aligned} \mathcal{L}_\pi(\theta_{k+1}) &= \mathbb{E}_{s \sim d_{\pi^{(k)}}} \left[D_{\text{KL}} \left[\pi^{(k)}(\cdot|s) \parallel \pi^{(k+1)}(\cdot|s) \right] \right], \\ \mathcal{L}_V(\theta_{k+1}) &= \mathbb{E}_{s \sim d_{\pi^{(k)}}} \left[\left(V^{(k)}(s) - V^{(k+1)}(s) \right)^2 \right]. \end{aligned} \quad (2)$$

The additional terms \mathcal{L}_{PG} and \mathcal{L}_{TD} are off-policy RL objectives for updating the actor and critic:

$$\begin{aligned} \mathcal{L}_{\text{PG}}(\theta_{k+1}) &= -\mathbb{E}_{s \sim d_{\pi^{(k)}}, a \sim \pi^{(k)}, s' \sim T(s, a)} \left[\log \pi^{(k+1)}(a|s) \perp \left(\frac{\pi^{(k+1)}(a|s)}{\pi^{(k)}(a|s)} A^{(k+1)}(s, a, s') \right) \right], \\ \mathcal{L}_{\text{TD}}(\theta_{k+1}) &= \mathbb{E}_{s \sim d_{\pi^{(k)}}, a \sim \pi^{(k)}, s' \sim T(s, a)} \left[\left(A^{(k+1)}(s, a, s') \right)^2 \perp \frac{\pi^{(k+1)}(a|s)}{\pi^{(k)}(a|s)} \right], \end{aligned} \quad (3)$$

where $A^{(k+1)}(s, a, s') = r(s, a) + \gamma \perp V^{(k+1)}(s') - V^{(k+1)}(s)$ denotes the estimated advantage of choosing action a and \perp is a **stop-gradient** operator, its operand is treated as a constant when taking derivatives of the objective. In practice, the losses in eq. (2) remain nonzero during distillation, potentially causing a drop in performance once the student replaces the teacher. The off-policy RL losses in eq. (3) allow the student to already take performance on the RL task into account, reducing or eliminating this performance drop. We use PPO losses to optimise eq. (3) in our experiments.

4.2 Combining Training and Distillation

One way to fully eliminate non-stationarity from the distillation phase is to collect the required data using a fixed teacher policy, after the previous RL training phase. However, not using this data to improve the teacher would increase the total number of environment interactions required. To improve sample efficiency, we consider two alternatives that reuse data between teacher *and* student:

1. *Sequential training*: Store the last N transitions that were used to update the teacher in a dataset \mathcal{D} . During the distillation phase, draw batches from \mathcal{D} instead of collecting new data from the environment. While this does not introduce non-stationarity, it leads to evaluating the teacher on old, off-policy data, for which the quality of its outputs may be degraded. The data might also be obsolete under the current state-distribution, possibly degrading the representation learned by the student. Lastly, memory is required to store \mathcal{D} .
2. *Parallel training*: Whenever the teacher is updated on a batch of data \mathcal{B} , also update the student on the same batch. \mathcal{B} could be drawn from a replay buffer or collected from the environment, depending on the base RL algorithm. This approach introduces some non-stationarity. However, the teacher typically changes less over the course of the distillation phase than a policy trained from scratch to achieve the same performance. This strategy guarantees that the teacher is only evaluated for data on which it is currently trained.

Both approaches perform similarly in our experimental validation. We use *parallel training* for the main experiments due to the smaller memory requirements and the ability to efficiently perform the additional computations required for the student distillation in parallel. Training the student through distillation typically requires significantly less data than training a similar policy using PPO, since the objective has much lower variance and the student does not need to re-explore the environment. This allows us to perform multiple distillation phases without prolonging the RL training. A schematic depiction of parallel ITER is given in fig. 1.

5 Experiments

In the following, we first re-visit the SL setting from section 3. Next, we evaluate ITER on the *Multi-room* [Chevalier-Boisvert and Willems, 2018] environment in section 5.2 and on several environments from the *ProcGen* [Cobbe et al., 2019a] benchmark in section 5.3. We also provide ablation studies showing that *parallel* and *sequential* training perform comparably, as well as that the addition of the loss terms eq. (3) in eq. (1) are beneficial.

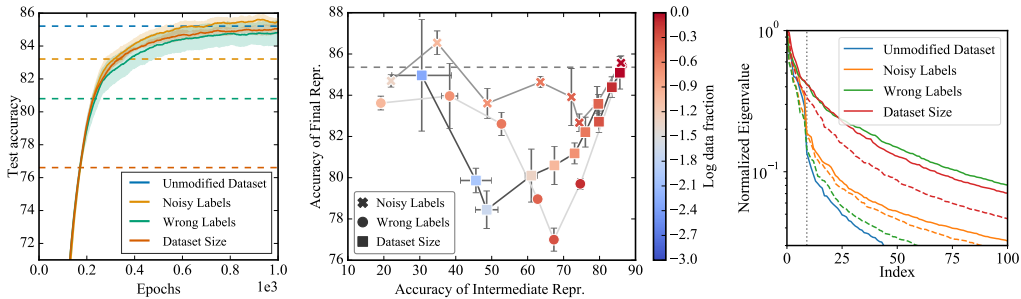


Figure 3: *Left:* Test accuracy of students (solid lines) that only learn to mimic the behaviour of poorly generalising teachers in fig. 2 (dashed lines). *Middle:* Final test accuracy of networks trained consecutively on two different datasets. The x -axis shows the accuracy of using encoders trained on the first dataset, retraining only the last layer on the second: nearly useless earlier representations impact future learning much less than slightly sub-optimal ones. Markers indicate modifications to first dataset; colours indicate the fraction of unmodified data points f . Dashed line shows accuracy for $f = 1$. *Right:* Singular values of feature matrix with rows $\phi(x)^T$. Solid lines show intermediate values of f with low test accuracy, dashed lines small values of f with higher accuracy. More plots can be found in the appendix.

5.1 Supervised Learning on CIFAR-10

Here, we revisit the SL setting presented in section 3. First, we confirm that it is possible to improve generalisation while only learning to mimic the outputs of a badly generalising teacher for the training data. We train the teacher using the same setup as in section 3, but only for 1500 epochs. As before, 1000 epochs use non-stationary data. We train a freshly initialised student for 1000 further epochs to fit the argmax predictions of this teacher on the training data, i.e., the labels in the training data are unused. Test accuracy is still measured using the true labels. The results of this distillation phase are shown in fig. 3 (left). Re-learning (solid lines) recovers the test accuracy achieved by training without non-stationarity, compared to the poor asymptotic teacher performance (dashed lines) from fig. 2.

Second, we aim to better understand the impact of non-stationarity on generalisation. We simplify the experimental setting to a two-phase setup. The first training phase uses a stationary, but modified, dataset $\mathcal{D}_{f,m}$, and the second phase uses the full dataset \mathcal{D} . To generate $\mathcal{D}_{f,m}$, we use the same modifications as before, $m \in \{\text{Noisy Labels}, \text{Wrong Labels}, \text{Dataset Size}\}$, but instead of annealing the fraction of correct data points from 0 to 1 as in section 3, it is fixed at the value f . We first train the network for 700 epochs on $\mathcal{D}_{f,m}$, which yields a representation $\phi_{f,m}$ (the activations of the network’s penultimate layer). We measure the usefulness of $\phi_{f,m}$ for the true task with the test accuracy of a linear predictor² that is trained for 800 epochs on the frozen representation $\phi_{f,m}$ of the full dataset \mathcal{D} . Next, we unfreeze $\phi_{f,m}$ and train for 800 epochs on the full data set \mathcal{D} . The final test accuracy shows how well the network can recover from the unfavourable initialisation.

In fig. 3 (middle), we plot the accuracy of the linear predictor on the x -axis and of the final network on the y -axis. Each point corresponds to one value of $f \in (0, 1]$ and one modification type indicated by the marker. Interestingly, having an almost useless representation after the first phase (30% on the x -Axis) does not impede subsequent learning much, but a slightly sub-optimal representation (around 60% on the x -axis) shows a clear dip in final performance for all data modifications. The dip is quite shallow for `Noisy Labels`, where generalisation suffers the least in section 3, but is substantial for `Wrong Labels` and `Dataset Size`. The comparatively good final performance for $f \rightarrow 0$ rules out decreased network flexibility, for example due to dead neurons (for ReLUs) or saturation (for tanh), as the main driver of reduced generalisation.

Our hypothesis is that the tendency of neural networks to find general features can be disrupted by *legacy features*, i.e., suboptimal features from earlier training, but *only if* these are sufficiently useful for the later training data. Otherwise, they do not interfere with training and can therefore be forgotten. If they are useful, instead of learning new features, the network reuses the existing ones. As these legacy features may have overfit to the early training data, relying on them may lead to worse generalisation. Due to the expressive power of neural networks, there is limited pressure to forget those legacy features: training data that is not captured well by less general legacy features can be memorised using additional features.

Consequently, in Figure 3 (right) we plot the singular values of the feature matrix $\Phi \in \mathbb{R}^{N \times p}$ for all $N = 10000$ test data points with rows corresponding to the features $\phi(x)^T \in \mathbb{R}^{1 \times p}$ that were trained on both datasets. We use both the smallest values of f (dashed lines) and those with the lowest test performance (solid lines, $f_{\text{noisy}} = 0.5$, $f_{\text{wrong}} = 0.5$, $f_{\text{size}} = 0.02$). All three non-stationarities lead to a spectrum with heavier tails, which are much more pronounced in the dips seen in the middle plot. This is consistent with our hypothesis that in these cases the network is required to learn *additional* features in the second phase to compensate for legacy features in the initial representation $\phi_{f,m}$.

5.2 Experimental Results on Multiroom

Next, we evaluate ITER on the *Multiroom* environment. The red agent’s task is to traverse a sequence of rooms to reach the goal (green square in fig. 4) as quickly as possible. It can take discrete actions to rotate 90° in either direction, move forward, and open or close the doors between rooms. The observation contains the *full* grid, one pixel per square. Object type, including empty space and walls, as well as any object status, like direction, are encoded in the three ‘colour’ channels. For each episode, a new layout is generated by randomly placing between one and four connected rooms on the grid. The agent is always initialised in the room furthest from the goal. This randomness favours agents that are better at generalising between layouts as memorisation is impossible due to the high

² The linear predictor is $y = \sigma(W\phi_{f,m}(x) + b)$, where σ is the softmax function and x the input image.

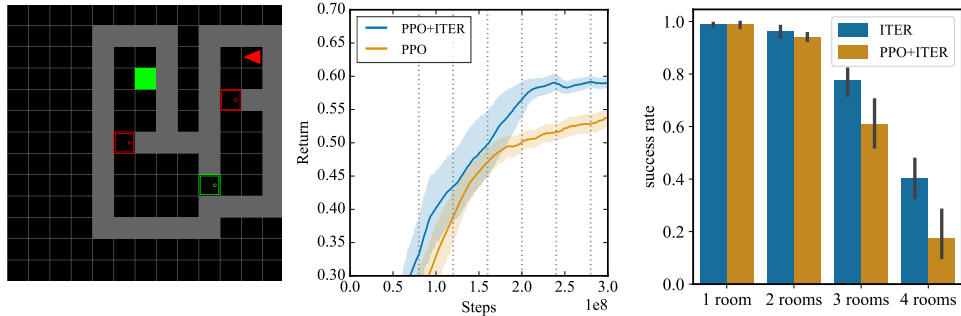


Figure 4: Evaluation on *Multiroom*. Shown are mean and standard error over twelve seeds. *Left:* Example layout. *Middle:* Return for PPO with and without ITER. Dotted lines indicate when the network was replaced by a new student. *Right:* Evaluation on layouts with a fixed number of rooms; training is still with a random number of rooms. ITER’s advantage is more pronounced for harder levels.

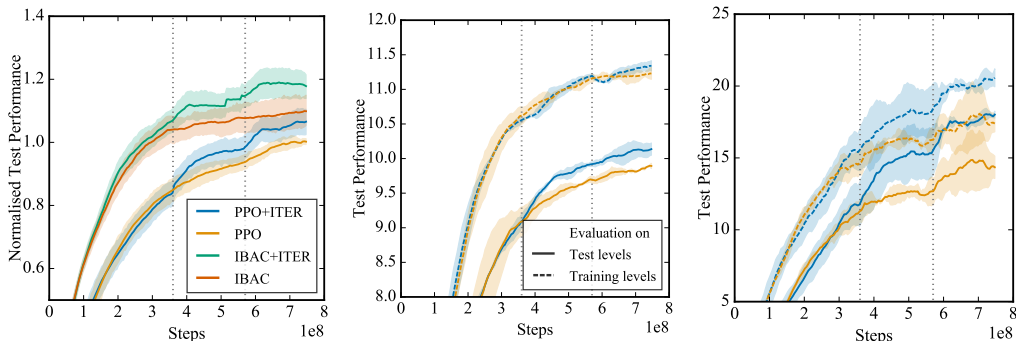


Figure 5: Evaluation on *ProcGen*. Dashed lines indicate replacing the teacher. *Left:* Test performance averaged over five environments (*StarPilot*, *Dodgeball*, *Climber*, *Ninja* and *BigFish*). Shown are mean and standard error over all ten runs (two per environment). Results are normalised by the final test-performance of the PPO baseline on each respective environment to make them comparable across environments. We also compare against the previous state of the art method Information Bottleneck Actor Critic (IBAC) with selective noise injection [Igl et al., 2019]. More plots can be found in the appendix. *Middle:* Evaluation on *Climber*. Note how ITER only improves test performance. *Right:* Evaluation on *BigFish*. ITER improves both train- and test- performance.

number of feasible layouts. The results are shown in fig. 4: Using ITER on top of PPO increases performance. The performance difference is more pronounced for layouts with more rooms, possibly because such layouts are harder and likely only solved later in training, at which point negative effects due to prior non-stationarity in training are more pronounced.

5.3 Experimental Results on ProcGen

Lastly, we evaluate ITER on several environments from the *ProcGen* benchmark. We follow the evaluation protocol proposed in [Cobbe et al., 2019a]: for each environment, we train on 500 randomly generated level layouts and test on additional, previously unseen levels. In difference to *Multiroom*, which suffers from a large state space but draws test episodes from the training distribution, the left out test levels in *ProcGen* exhibit states that have not been seen during training. Due to computational constraints, we consider a subset of five environments. We chose *StarPilot*, *Dodgeball*, *Climber*, *Ninja*, and *BigFish* based on the results presented in [Cobbe et al., 2019a] as they showed baseline generalisation performance better than a random policy, but with a large enough generalisation gap. ITER improves performance for both PPO and IBAC with selective noise injection [Igl et al., 2019]. Results are presented in fig. 5 and more individual plots

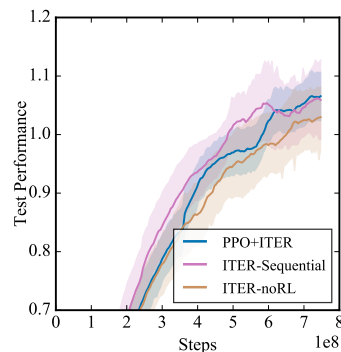


Figure 6: Ablation studies with sequential ITER and ITER without terms \mathcal{L}_{PG} and \mathcal{L}_{TD} (eq. (3)).

can be found in the appendix. In fig. 6 we show in ablations that both the parallel and sequential implementations of ITER perform comparably, while not using the off-policy RL terms \mathcal{L}_{PG} and \mathcal{L}_{TD} in eq. (1) slightly decreases performance.

Similarly to previous literature [Cobbe et al., 2019b, Igl et al., 2019], we found that weight decay improves performance and apply it to all algorithms evaluated on *ProcGen*. Our results show that the negative effects of non-stationarity cannot easily be avoided through standard network regularisation: we can improve test returns through ITER despite regularisation with weight decay and IBAC, both shown to be among the most effective regularisation methods on this benchmark [Igl et al., 2019].

6 Related Work

Knowledge distillation [Hinton et al., 2015] with identical teacher and student architectures has been shown to improve test accuracy [Furlanello et al., 2018], even in the absence of non-stationarities in the data. This improvement has been attributed to the ease of predicting the output *distribution* of the teacher compared to the original ‘hard’ labels [Mobahi et al., 2020, Gotmare et al., 2019]. While we apply such ‘soft’ distillation for ITER on RL, we use ‘hard’ labels in our SL experiments to show that distillation can even then improve performance when used on a stationary data distribution.

Policy distillation has been applied to RL [Czarnecki et al., 2019], for example for multi-task learning and compression [Teh et al., 2017, Rusu et al., 2015, Parisotto et al., 2016], imitation learning [Ross et al., 2011], or faster training [Schmitt et al., 2018, Ghosh et al., 2018]. Closer to ITER, Czarnecki et al. [2018] use policy distillation to learn a *sequence* of agents. However, their Mix & Match algorithm solves tasks of growing complexity, for example, to grow the action space of the agent, not to tackle generalisation or non-stationarity.

While the topic of non-stationarity is central to the area of continual learning (see [Parisi et al., 2019] for a recent review), the field is primarily concerned with preventing catastrophic forgetting [French, 1999] when the environment or task changes *during training* [Li and Hoiem, 2017, Schwarz et al., 2018]. For non-stationary environments *during agent deployment*, the approach is typically to detect such changes and respond accordingly [Choi et al., 2000, Da Silva et al., 2006, Doya et al., 2002]. By contrast, we assume a stationary environment and investigate the impact of non-stationarity induced by an improving policy and value function bootstrapping. We also show that intentionally forgetting the representation, but not the learned outputs, can improve generalisation in this case.

Neural networks are used in deep RL to allow generalisation across similar states [Sutton and Barto, 2018]. Several possibilities have been proposed to further improve generalisation, including to provide more diverse training environments [Tobin et al., 2017], inject noise into the environment [Stulp et al., 2011, Lee et al., 2020], incorporate inductive biases in the architecture [Kansky et al., 2017], or regularise the network [Cobbe et al., 2019b, Igl et al., 2019, Liu et al., 2019]. While regularisation reduces overfitting, we show in our experiments that this is insufficient to counter the negative effects of non-stationarity, and that ITER can be complementary to other types of regularisation.

7 Conclusion

In this work, we investigate the impact of non-stationarity on the generalisation performance of trained RL agents. First, in several SL experiments on the CIFAR-10 dataset, we confirm that non-stationarity can considerably degrade test performance while leaving training performance nearly unchanged. To explain this effect, we propose and experimentally support the *legacy feature* hypothesis that networks exhibit a tendency to adopt, rather than forget, features learned earlier during training *if* they are sufficiently relevant, though not necessarily optimal, for the new data. We also show that self-distillation, even without using the true training labels, improves performance on the test-data.

We highlight that many deep RL training algorithms induce non-stationarities similar to those we investigate on CIFAR-10, for example due to a gradually improving policy and subsequent changes to the observed state-distribution. To improve generalisation in deep RL, we propose ITER which reduces the non-stationarity the agent experiences during training. Our experimental results on the *Multiroom* and *ProcGen* benchmarks show that ITER improves generalisation, even in addition to strong regularisation methods.

Broader Impact

We hope our findings are of use both to improve our understanding of how networks learn and to improve generalisation in RL in particular. Generalisation is important for many applications of RL since the number of situations a deployed agent can encounter can vastly exceed the number of (even approximate) states that can be feasibly observed during training. One obvious example is autonomous driving, where weather, lighting, traffic participants, and other objects can always create new, unique situations. As a result, deploying learned RL agents outside of simulations often suffers from a large *generalisation gap*, i.e., lower performance in deployment than during training. If RL agents control important systems, poor generalisation can lead to dangerous errors. Conversely, if they generalise well RL agents can be deployed safely and effectively in more contexts.

In deep RL we rely on neural networks to generalise. Unfortunately, much about how or why neural networks generalise is still unknown. In this work, we both advance our understanding of the generalisation problem in deep RL, and propose an algorithmic approach to improve generalisation. This line of work may help us realise the potential benefits of RL agents, which may be able to perform useful tasks or aid human decision makers in solving difficult problems. Of course, there are many other challenges in building safe and useful RL agents, such as specifying reward functions that align well with intended behaviours. Furthermore, improved generalisation in a simulated environment should not give over-confidence that agents will generalise well to dramatically different states (such as from simulation to the real world, or from one real world setting to another). Lastly, without a thorough theoretical understanding of how neural networks learn to generalise, it is impossible to know under which constraints improvements due to ITER can be guaranteed, if at all. We hope that our experiments prove to be helpful for further advances in this direction, but much work remains to be done.

References

- M. Chevalier-Boisvert and L. Willems. Minimalistic gridworld environment for openai gym. <https://github.com/maximecb/gym-minigrid>, 2018.
- S. P. Choi, D.-Y. Yeung, and N. L. Zhang. An environment model for nonstationary reinforcement learning. In *Advances in neural information processing systems*, pages 987–993, 2000.
- K. Cobbe, C. Hesse, J. Hilton, and J. Schulman. Leveraging procedural generation to benchmark reinforcement learning. *arXiv preprint arXiv:1912.01588*, 2019a.
- K. Cobbe, O. Klimov, C. Hesse, T. Kim, and J. Schulman. Quantifying generalization in reinforcement learning. In *Proceedings of the 36th International Conference on Machine Learning*, 2019b.
- W. Czarnecki, S. Jayakumar, M. Jaderberg, L. Hasenclever, Y. W. Teh, N. Heess, S. Osindero, and R. Pascanu. Mix & match agent curricula for reinforcement learning. In *International Conference on Machine Learning*, pages 1087–1095, 2018.
- W. M. Czarnecki, R. Pascanu, S. Osindero, S. M. Jayakumar, G. Swirszcz, and M. Jaderberg. Distilling policy distillation. *arXiv preprint arXiv:1902.02186*, 2019.
- B. C. Da Silva, E. W. Basso, A. L. Bazzan, and P. M. Engel. Dealing with non-stationary environments using context detection. In *Proceedings of the 23rd international conference on Machine learning*, pages 217–224, 2006.
- K. Doya, K. Samejima, K.-i. Katagiri, and M. Kawato. Multiple model-based reinforcement learning. *Neural computation*, 14(6):1347–1369, 2002.
- L. Espeholt, H. Soyer, R. Munos, K. Simonyan, V. Mnih, T. Ward, Y. Doron, V. Firoiu, T. Harley, I. Dunning, et al. Impala: Scalable distributed deep-rl with importance weighted actor-learner architectures. *arXiv preprint arXiv:1802.01561*, 2018.
- J. Frankle, D. J. Schwab, and A. S. Morcos. The early phase of neural network training. In *International Conference on Learning Representations*, 2020. URL <https://openreview.net/forum?id=Hk11iRNFwS>.

- R. M. French. Catastrophic forgetting in connectionist networks. *Trends in cognitive sciences*, 3(4): 128–135, 1999.
- T. Furlanello, Z. Lipton, M. Tschannen, L. Itti, and A. Anandkumar. Born again neural networks. In *International Conference on Machine Learning*, pages 1607–1616, 2018.
- D. Ghosh, A. Singh, A. Rajeswaran, V. Kumar, and S. Levine. Divide-and-conquer reinforcement learning. In *International Conference on Learning Representations*, 2018. URL <https://openreview.net/forum?id=rJwElMbR->.
- A. S. Golatkar, A. Achille, and S. Soatto. Time matters in regularizing deep networks: Weight decay and data augmentation affect early learning dynamics, matter little near convergence. In *Advances in Neural Information Processing Systems*, pages 10677–10687, 2019.
- A. Gotmare, N. S. Keskar, C. Xiong, and R. Socher. A closer look at deep learning heuristics: Learning rate restarts, warmup and distillation. In *International Conference on Learning Representations*, 2019. URL <https://openreview.net/forum?id=r14E0sCqKX>.
- K. He, X. Zhang, S. Ren, and J. Sun. Deep residual learning for image recognition. In *Proceedings of the IEEE conference on computer vision and pattern recognition*, pages 770–778, 2016.
- G. Hinton, O. Vinyals, and J. Dean. Distilling the knowledge in a neural network. *arXiv preprint arXiv:1503.02531*, 2015.
- M. Igl, K. Ciosek, Y. Li, S. Tschitschek, C. Zhang, S. Devlin, and K. Hofmann. Generalization in reinforcement learning with selective noise injection and information bottleneck. In *Advances in Neural Information Processing Systems*, pages 13956–13968, 2019.
- K. Kansky, T. Silver, D. A. Mély, M. Eldawy, M. Lázaro-Gredilla, X. Lou, N. Dorfman, S. Sidor, S. Phoenix, and D. George. Schema networks: Zero-shot transfer with a generative causal model of intuitive physics. In *Proceedings of the 34th International Conference on Machine Learning-Volume 70*, pages 1809–1818. JMLR. org, 2017.
- R. Kemker, M. McClure, A. Abitino, T. L. Hayes, and C. Kanan. Measuring catastrophic forgetting in neural networks. In *Thirty-second AAAI conference on artificial intelligence*, 2018.
- A. Krizhevsky, G. Hinton, et al. Learning multiple layers of features from tiny images. 2009.
- K. Lee, K. Lee, J. Shin, and H. Lee. Network randomization: A simple technique for generalization in deep reinforcement learning. In *International Conference on Learning Representations*, 2020. URL <https://openreview.net/forum?id=HJgcvJBFvB>.
- Z. Li and D. Hoiem. Learning without forgetting. *IEEE transactions on pattern analysis and machine intelligence*, 40(12):2935–2947, 2017.
- Z. Liu, X. Li, B. Kang, and T. Darrell. Regularization matters in policy optimization. *arXiv preprint arXiv:1910.09191*, 2019.
- H. Mobahi, M. Farajtabar, and P. L. Bartlett. Self-distillation amplifies regularization in hilbert space. *arXiv preprint arXiv:2002.05715*, 2020.
- G. I. Parisi, R. Kemker, J. L. Part, C. Kanan, and S. Wermter. Continual lifelong learning with neural networks: A review. *Neural Networks*, 2019.
- E. Parisotto, J. Ba, and R. Salakhutdinov. Actor-mimic: Deep multitask and transfer reinforcement learning. In *5th International Conference on Learning Representations, ICLR 2016*, 2016.
- M. L. Puterman. *Markov decision processes: discrete stochastic dynamic programming*. John Wiley & Sons, 2014.
- S. Ross, G. Gordon, and D. Bagnell. A reduction of imitation learning and structured prediction to no-regret online learning. In *Proceedings of the fourteenth international conference on artificial intelligence and statistics*, pages 627–635, 2011.

- A. A. Rusu, S. G. Colmenarejo, C. Gulcehre, G. Desjardins, J. Kirkpatrick, R. Pascanu, V. Mnih, K. Kavukcuoglu, and R. Hadsell. Policy distillation. *arXiv preprint arXiv:1511.06295*, 2015.
- S. Schmitt, J. J. Hudson, A. Zidek, S. Osindero, C. Doersch, W. M. Czarnecki, J. Z. Leibo, H. Kuttler, A. Zisserman, K. Simonyan, et al. Kickstarting deep reinforcement learning. *arXiv preprint arXiv:1803.03835*, 2018.
- J. Schulman, F. Wolski, P. Dhariwal, A. Radford, and O. Klimov. Proximal policy optimization algorithms. *arXiv preprint arXiv:1707.06347*, 2017.
- J. Schwarz, J. Luketina, W. M. Czarnecki, A. Grabska-Barwinska, Y. W. Teh, R. Pascanu, and R. Hadsell. Progress & compress: A scalable framework for continual learning. *arXiv preprint arXiv:1805.06370*, 2018.
- B. Settles. Active learning literature survey. Technical report, University of Wisconsin-Madison Department of Computer Sciences, 2009.
- F. Stulp, E. Theodorou, J. Buchli, and S. Schaal. Learning to grasp under uncertainty. In *2011 IEEE International Conference on Robotics and Automation*, pages 5703–5708. IEEE, 2011.
- R. S. Sutton. Learning to predict by the methods of temporal differences. *Machine learning*, 3(1): 9–44, 1988.
- R. S. Sutton and A. G. Barto. Reinforcement learning: An introduction. 2018.
- Y. Teh, V. Bapst, W. M. Czarnecki, J. Quan, J. Kirkpatrick, R. Hadsell, N. Heess, and R. Pascanu. Distal: Robust multitask reinforcement learning. In *Advances in Neural Information Processing Systems*, pages 4496–4506, 2017.
- J. Tobin, R. Fong, A. Ray, J. Schneider, W. Zaremba, and P. Abbeel. Domain randomization for transferring deep neural networks from simulation to the real world. In *2017 IEEE/RSJ International Conference on Intelligent Robots and Systems (IROS)*, pages 23–30. IEEE, 2017.

A Pseudo code

Algorithm 1: Pseudo-Code for parallel ITER

```

1 Input Length of initial RL training phase  $t_{init}$ , length of distillation phase  $t_{distill}$ 
2 Initialise  $k \leftarrow 0$ , policy  $\pi^{(k)}$ , value function  $V^{(k)}$ 
3 // Normal RL training at the beginning
4 for  $t_{init}$  steps do
5    $\mathcal{B} \leftarrow$  collect trajectory data using  $\pi^{(0)}$ 
6   Update  $\pi^{(0)}$  and  $V^{(0)}$  using standard RL method using  $\mathcal{B}$ 
7 // Combine further RL training of  $\pi^{(k)}$ ,  $V^{(k)}$  with distillation of  $\pi^{(k+1)}$ ,  $V^{(k+1)}$ 
8 while not converged do
9   Initialise student policy  $\pi^{(k+1)}$  and value function  $V^{(k+1)}$ 
10  for  $t_{distill}$  steps do
11     $\alpha_V, \alpha_\pi \leftarrow$  linear annealing to 0 over  $t_{distill}$  steps
12     $\mathcal{B} \leftarrow$  collect trajectory data using  $\pi^{(k)}$ 
13    Update  $\pi^{(k)}$  and  $V^{(k)}$  with standard RL method using  $\mathcal{B}$ 
14    Update  $\pi^{(k+1)}$  and  $V^{(k+1)}$  with eq. (1) using  $\mathcal{B}$ ,  $\alpha_V$ ,  $\alpha_\pi$ ,  $\pi^{(k)}$  and  $V^{(k)}$ 
15  // Housekeeping
16  Discard  $\pi^{(k)}$  and  $V^{(k)}$ 
17  Set  $k \leftarrow k + 1$ 

```

B Supervised Learning

Table 1: Numerical values of results presented in fig. 2. The ‘Rel’ column shows the error normalised by the error of the unmodified dataset. The error on the test-data deteriorates worse than on the training data, not only in absolute, but also relativ terms.

	Training		Testing	
	Error in %	Rel.	Error in %	Rel.
Unmodified	0.17 ± 0.09	1.0	14.8 ± 0.70	1.0
Noisy Labels	0.19 ± 0.09	1.13	16.8 ± 0.70	1.14
Wrong Labels	0.20 ± 0.08	1.22	19.2 ± 0.43	1.30
Dataset Size	0.18 ± 0.08	1.05	23.4 ± 0.83	1.58

Table 2: Hyper-parameters used in the supervised learning experiment on CIFAR-10

Hyper-parameter	Value
SGD: Learning rate	3×10^{-4}
SGD: Momentum	0.9
SGD: Weight decay	5×10^{-4}

Here we provide additional training details and results for the supervised learning experiments performed on the CIFAR-10 dataset. We used a ResNet18 architecture without Batchnorm, hyper-parameters for the SGD optimiser are given in table 2. In table 1 we provide exact numerical values for the results in fig. 2. We also provide values for the *relative* change in error rate due to the introduction of non-stationarities, for which the test-performance is also more affected than the train performance.

In fig. 7, we show the same results as in fig. 3, but here showing the f values used to generate $\mathcal{D}_{f,m}$ on the x-Axis. The same ‘dips’ in performance are visible, however from this figure it is clear that Dataset Size experiences it for

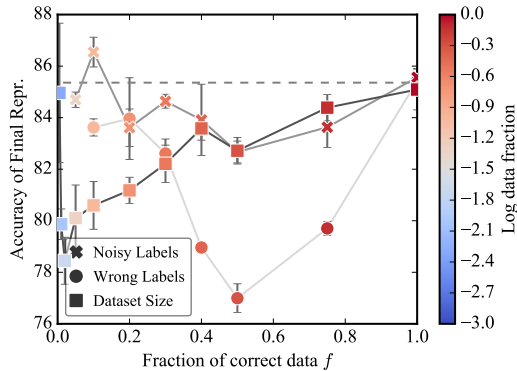


Figure 7: Same results as in fig. 3 (middle), but with the fraction of correct data points f on the x-Axis

much smaller values of f , which is unsurprising, giving the missing influences of a diverse input-data distribution.

Lastly, in fig. 8, we provide the individual training runs used to generate fig. 3(middle) and fig. 7.

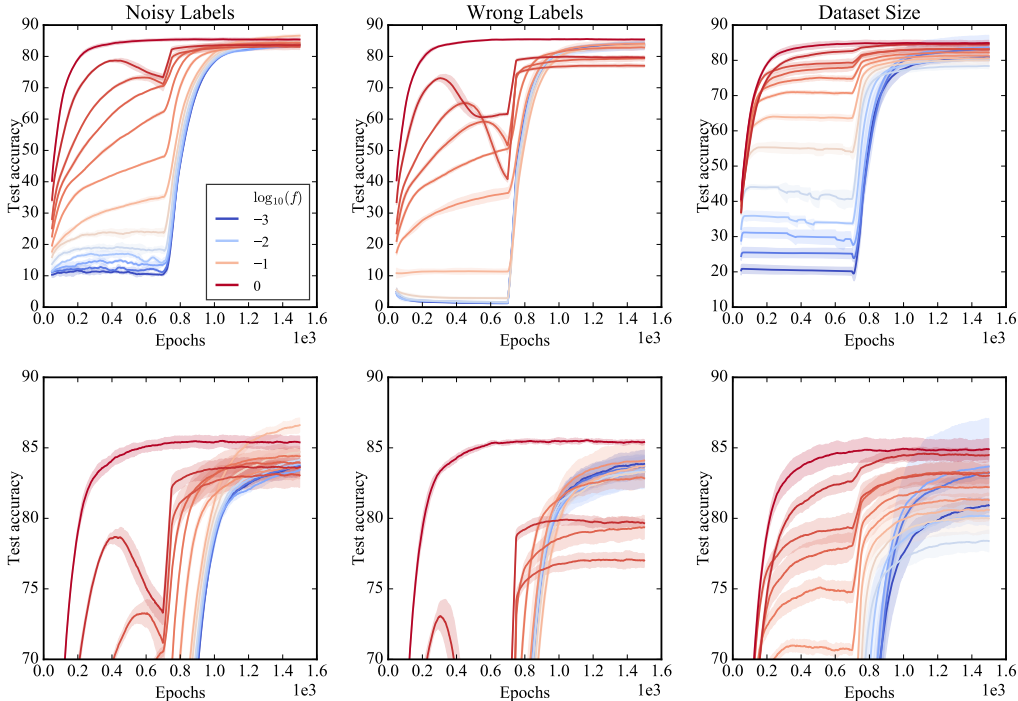


Figure 8: Individual training curves for the data used in fig. 3(middle) and fig. 7. The bottom row shows the same data as the top row, just ‘zoomed in’.

B.1 Multiroom

In table 3 we show the hyper-parameters used for the Multiroom experiments which are shared between ‘PPO’ and ‘PPO+ITER’. We note that our Multiroom environment uses the same modification that was used in [Igl et al., 2019] to make the environment fully observable. In the original environment, the agent only observed its immediate surrounding from an ego-centric perspective, thereby naturally generalising across various layouts. Instead, full observability introduces the need to *learn* how to generalise. Our network consists of a three layer CNN With 16, 32 and 32 filters respectively, followed by a fully connected layer of size 64. One max-pooling layer is used after the first CNN layer. We use $t_{init} = 4 \times 10^7$ and $t_{distill} = 4 \times 10^7$ (see algorithm 1) for the duration of the initial RL training phase and the following distillation phases.

B.2 ProcGen

In fig. 9 we show all results on the various *ProcGen* environment from which the summary plots in the main text (figs. 5 and 6) are computed. We use the same (small) IMPALA architecture as used by [Cobbe et al., 2019b]. Training is done on 4 GPUs in parallel. One GPU is continuously evaluating the test performance, the other three are used for training. Their gradients are averaged at each update step. The hyper-parameters given in table 4 are *per GPU*. The x -Axis in fig. 9 shows the total number of consumed frames, i.e. 250×10^6 per *training GPU*. The distillation phase takes $t_{distill} = 70 \times 10^6$ frames (again per GPU) and we linearly anneal α_π from 1 to 0 and α_V from 0.5 to 1. The values of α_π and α_V were chosen to reflect the relative weight between \mathcal{L}_{PG} and \mathcal{L}_{TD} in eq. (1) and no further tuning was done. The initial RL training phase takes $t_{init} = 50 \times 10^6$ frames. The distillation length was chosen based on preliminary experiments on *BigFish* by increasing its length in steps of 10×10^6 frames until no drop in training performance was experienced when switching to a new student.

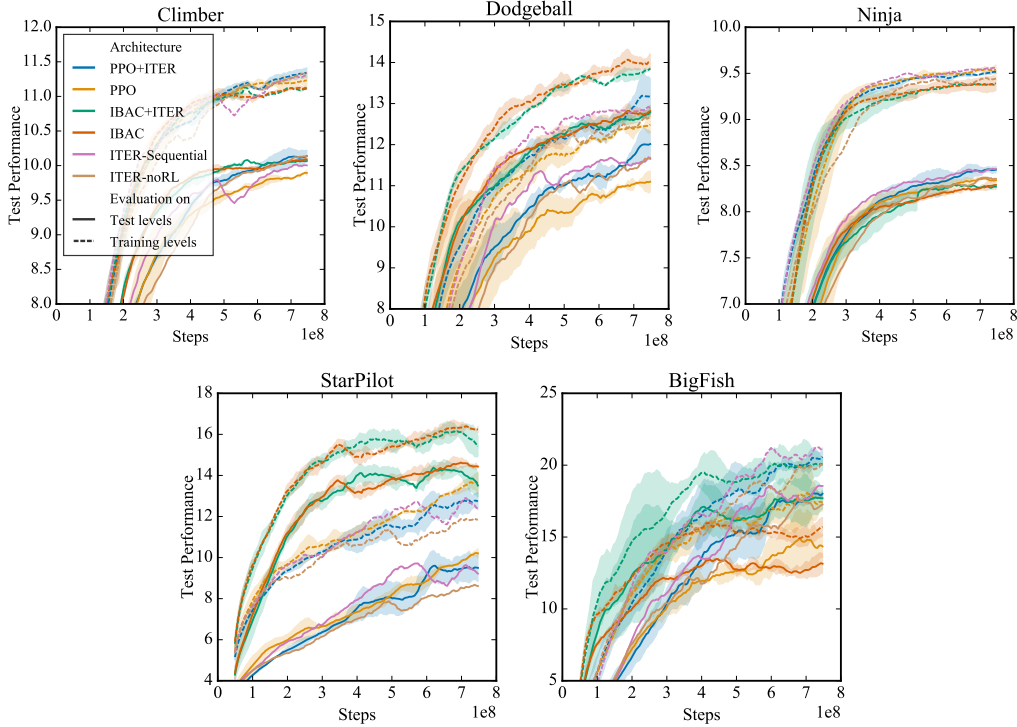
Table 3: Hyper-parameters used for Multiroom

Hyper-parameter	Value
PPO: $\lambda_{\text{Entropy Loss}}$	0.01
PPO: λ_{TD}	0.5
PPO: ϵ_{Clip}	0.2
PPO Epochs	4
PPO Minibatch Size	2048
Parallel Environments	32
Frames per Env per Update	256
λ_{GAE}	0.95
γ	0.99
Adam: Learning rate	7×10^{-4}
Adam: ϵ	1×10^{-5}

Table 4: Hyper-parameters used for ProcGen

Hyperparameter	Value
PPO: $\lambda_{\text{Entropy Loss}}$	0.01
PPO: λ_{TD}	0.5
PPO: ϵ_{Clip}	0.2
PPO Epochs	3
PPO Nr. Minibatches	8
Parallel Environments	64
Frames per Env per Update	256
λ_{GAE}	0.95
γ	0.999
Adam: Learning rate	5×10^{-4}
Adam: ϵ	1×10^{-5}
Adam: Weight decay	1×10^{-4}

Due to the high computation costs of running experiments on the *ProcGen* environment (4 GPUs for about 24h for each run), we decided to exclude environments from the original benchmark based on results presented by Cobbe et al. [2019a], figures 2 and 4. We excluded environments for two different reasons, either because the generalisation gap was small (Chaser, Miner, Leaper, Boss Fight, Fruitbot) or because generalisation did not improve at all during training after a very short initial jump (CaveFlyer, Maze, Heist, Plunder, Coinrun), indicating that either it was too hard, or a very simple policy already achieved reasonable performance.

**Figure 9:** All individual results on *ProcGen*. Shown is the mean and standard deviation across two random seeds.